Available online at www.sciencedirect.com
SCIENCE DIRECT
Earth and Planetary Science Letters 236 (2005) 732–750
EPSL
www.elsevier.com/locate/epsl

Gravity anomalies, flexure and the elastic thickness structure of the India–Eurasia collisional system

T.A. Jordan *, A.B. Watts

Department of Earth Sciences, University of Oxford, Parks Road, Oxford, OX1 3PR, U.K.

Received 18 November 2004; received in revised form 9 May 2005; accepted 23 May 2005

Editor: V. Courtillot

Abstract

We have used Bouguer gravity anomaly and topography data to determine the equivalent elastic thickness of the lithosphere, T_e in the region of the India–Eurasia collisional system. Comparison of observed and modelled gravity anomalies along 1-dimensional profiles suggest there are significant variations in T_e along-strike of the Himalaya foreland. Estimates decrease from a high of 70 km in the central region to 30–50 km in the east and west. We have verified these inferences of spatial variations using a 2-dimensional, non-spectral, interative flexure and gravity anomaly modelling technique. The Himalaya foreland forms a high T_e ($40 < T_e < 100$ km) rigid block with a well defined edge, as shown by the localisation of faulting and deformation along its northern margin. Other high T_e blocks occur to the north beneath the Qaidam and Sichuan basins. The Tibetan plateau forms a low T_e ($0 < T_e < 20$ km) weak region that extends from the central part of the plateau into south-western China. Tectonic styles in the India–Eurasia collisional system therefore involve both 'rigid' and 'non-rigid' blocks. Where high T_e rigid blocks are present the styles dominated by underthrusting of the more rigid block. Where the collisional zone is not constrained by rigid blocks, however, the style appears to be dominated by lower crustal flow and a more continuous style of deformation.

Keywords: elastic thickness; flexure; isostasy; tectonics

1. Introduction

The flexural rigidity, as determined by the equivalent elastic thickness, T_e provides a measure of the long-term strength of the lithosphere. Previous studies suggest continental T_e is in the range 5 to 125 km (see summary in Watts 2001 [1]) with the highest values being associated with cratonic shields and the lowest values with extensional rift-type basins. Recently, McKenzie and Fairhead [2] have questioned the validity of continental T_e values >25 km, especially those based on the Bouguer coherence spectral technique (e.g., [3–5]).

The controversy has focussed on the India–Eurasia collisional system in the region of the Himalayan foreland. Lyon-Caen and Molnar [6] and Karner and Watts [7], for example, used forward modelling techniques to

* Corresponding author.
E-mail address: tomj@earth.ox.ac.uk (T.A. Jordan).

0012-821X/$ - see front matter © 2005 Elsevier B.V. All rights reserved.
doi:10.1016/j.epsl.2005.05.036

show that the Bouguer gravity anomaly over the Ganges basin could be explained by the flexure of the Indian continental lithosphere. They modelled the flexure by applying forces that were representative of the load of the Himalaya and Tibetan plateau on the end of an elastic beam that overlies an inviscid fluid. By comparing the observed gravity data to model predictions they showed that T_e of the continental lithosphere was in the range 80–110 km [6,7]. McKenzie and Fairhead [2], however, challenged these high values using spectral estimates of the free-air admittance and a non-spectral free-air gravity anomaly profile shape-fitting technique. They concluded that the T_e of Indian lithosphere was low (24 km by admittance and 42 km by shape-fitting) and significantly less than that obtained by previous workers.

The low values derived by McKenzie and Fairhead [2] are of the order of the thickness of the seismogenic layer, T_s which is the depth range over which earthquakes occur [8]. This led Jackson [9,10] to question earlier rheological models of a strong upper crust, weak lower crust and strong mantle proposed, for example, by Chen and Molnar [11]. They proposed instead a single strong crustal layer that 'floated' on an underlying weak, non-seismogenic, mantle.

The inference that a lack of earthquakes implies a weak mantle has subsequently been questioned. Watts and Burov [12], for example, suggest that tectonic stresses (including those associated with flexure) are not usually large enough to exceed the brittle strength of the sub-crustal mantle and generate earthquakes. Handy and Brun [13] also dispute the link between the presence or absence of earthquakes and the long-term strength of the lithosphere. Based on structural and laboratory-based studies of the deep-structure of orogens and rifted margins, they argue that the mantle must be strong. These studies suggest therefore that rather than being equal to T_s, T_e may very well exceed it.

Since McKenzie and Fairhead [2], there have been a number of forward modelling (e.g., [14]) and spectral (e.g., [15–19]) studies of the India–Eurasia collisional system. These yield T_e values in the range 10–50 km. Forward modelling along profiles [14] yield a single estimate of T_e as do spectral methods based on profiles [14] and windows of fixed sizes [16–18]. Only Rajesh and Mishra [19] directly considered the possibility of spatial variations in rigidity by calculating the spectral estimates in multiple, overlapping, windows. Rather than considering the actual values of T_e however, Rajesh and Mishra [19] expressed the variations in terms of spatial changes in the Bouguer coherence transitional wavelength.

Spectral studies of continent-wide gravity anomaly and topography data elsewhere (e.g., North America—[20–22], South America—[5], Africa—[23], Fennoscandia—[24]) suggest that T_e of cratonic regions is high and >~60 km. However, as Perez et al. [24] have recently shown, there are difficulties with the spectral estimation of T_e. One problem is that the ability to recover high T_e is dependant on window size. If the region of high T_e is of small areal extent, relative to the window, a lower average T_e may be recovered. Smaller window sizes will improve the resolution, but may not be large enough to recover the maximum value of T_e.

An alternative approach, which avoids some of the problems with spectral methods, has been suggested by Braitenberg et al. [25]. These workers use the surface topographic load to calculate the flexure of the top and bottom of the crust for a range of uniform T_e values. The T_e which gives the best fit between an observed Moho, derived from gravity and seismic data, and the flexed Moho within a window is then assigned to its centre. By moving the window stepwise across the Tibetan plateau, Braitenberg et al. [25] recovered a T_e structure that varied from 8 to 110 km over horizontal distances of less than 250 km. They found that the lowest values of T_e occurred in the centre of the plateau and the highest over flanking regions.

The purpose of this paper is to use both forward and non-spectral inverse gravity modelling techniques to determine the T_e structure of the India–Eurasia collisional system. The study is carried out in 3 main steps. First, we use forward modelling to show that the centre of the Himalaya foreland has a high T_e ($\approx$70 km) while regions to the east and west have lower values ($\approx$30–50 km). Then, an inverse technique, which synthetic modelling shows is capable of recovering a high resolution T_e structure *directly* from gravity anomaly and topography data, is used to verify these T_e variations. Finally, we examine the implications of the T_e structure for the terrane structure of peninsula India and for tectonic processes in the Tibetan plateau and surrounding regions.

2. Geological setting

The India—Eurasia plate boundary is one of the best-known examples of continent continent collision on Earth. The collisional process has created the Himalayan mountains with many peaks over 7000 m and the Tibetan plateau which, in places, is over 1000 km wide and 3000 m high. The collision culminated during the Eocene (~50 Ma) when the Indian plate underthrust the southern margin of Eurasia. Paleomagnetic evidence suggests that during the Cenozoic, India 'indented' Eurasia by as much as ~2000 km [26]. In the process, the crust has thickened to ~70 km below the Tibetan plateau and deformation has been distributed across a 1500 km wide region to the north of the Indian plate.

3. Gravity anomaly and topography profiles

Most previous studies of T_e in collisional systems have been based on profiles and vertical end loads and/or moments applied to the end of a semi-infinite (i.e., broken) plate (e.g., [7]). The plate break was varied, together with T_e so as to achieve a best fit between observed and calculated Bouguer gravity anomaly profile data. More recent studies use the actual topography and either a finite difference (e.g., [27]) or a finite element model (e.g.,[14]) to simulate the plate break.

We follow here the approach of Stewart and Watts [27] in which the 1-dimensional finite difference method of Bodine [28] is used to calculate the flexure and the line integral method of Bott [29] is used to calculate the resulting gravity anomalies. We consider the load to comprise of two parts: a "driving load" given by the topography (above sea-level) between the mountain front and the plate break and an "infill load" given by the material which fills in the flexure. Both the driving and infill loads contribute, of course, to the flexure so that if they were removed due, for example, to erosion, then the flexed plate would return to its equilibrium, unloaded and stress-free state.

van Wees and Cloetingh [30] suggested that the original formulation of Bodine [28] may not be correct because of his omission of certain cross-terms in the general flexure equation. We therefore computed the flexure using the Bodine method and compared it with the analytical solutions of Hetényi [31]. We considered a 5 km high, 200 km wide rectangular load with one edge on the end of a broken elastic plate with T_e=90 km and other parameters as defined in Table 1. The plate break was simulated by a T_e that increased from 0 to 90 km over the first 100 km of the profile. The finite difference method gave a value of 20.28 km for the deflection at the plate break while the analytical solution showed the maximum flexure to be 19.67 km. The two methods are therefore in close agreement. The T_e used in the finite difference model that best fit (i.e., minimum Root Mean Square (RMS)) the analytical solution was 93 km which is only 3.3% higher. The flexure computed using the two methods is therefore in close agreement, suggesting a T_e that increases from zero to a high value over a short distance is a satisfactory way to simulate one end of a broken plate.

The profile method used in this study differs from that of McKenzie and Fairhead [2] and McKenzie [32]. We assume the load and the plate break, and then calculate the flexure and hence, the Bouguer anomaly for different values of T_e. The best fit T_e and the position of the plate break is then selected as the one that minimises the RMS difference between observed and calculated Bouguer anomalies. Synthetic tests show that this method recovers well both the T_e and the position of the plate break (Fig. A1). McKenzie and Fairhead [2], in contrast, used a curve-fitting technique to recover T_e directly from the shape of the observed free-air anomaly, thereby avoiding the need to make assumptions about the load and plate break. Both methods are based on the gravity anomaly and should yield sim-

Table 1
Parameters assumed in the flexure and gravity modelling

Parameter	Value
Poisson ratio	0.25
Young's modulus	10^{11} Pa
Crustal density	2800 kg m^{-3}
Mantle density	3330 kg m^{-3}
Infill density	2650 kg m^{-3}
Load density	2650 kg m^{-3}

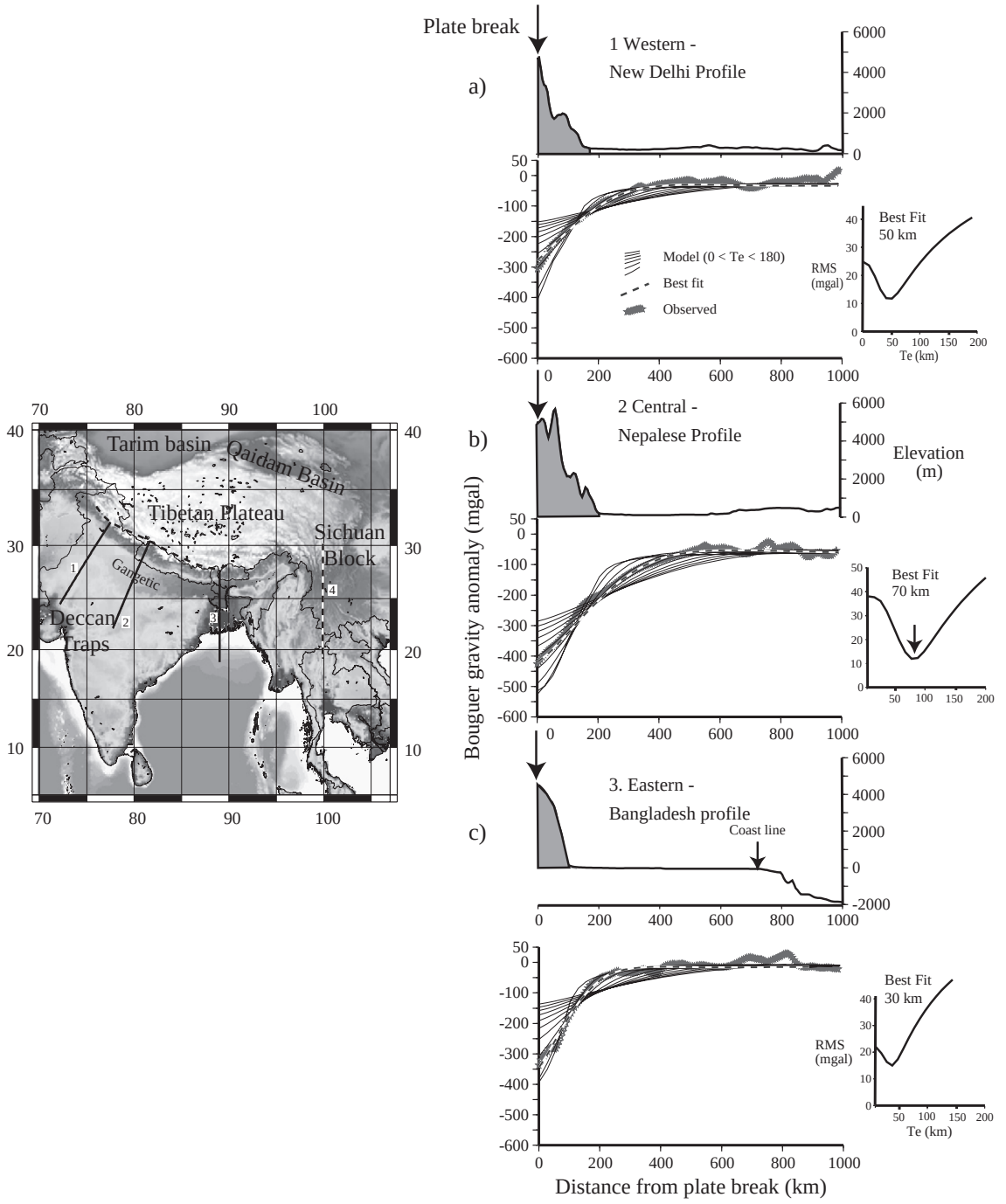

Fig. 1. Location map and observed and calculated Bouguer gravity anomaly profiles of the Himalaya foreland region. The map is based on a GETECH '5 × 5' minute grid [69]. Thick solid lines show the location of the eastern, central and western profiles. Thin dashed line shows the location of the additional profile in Fig. 6. Thick dashed line shows the position of the 'best fit' plate break. a) Western profile. The upper profile shows topography. The lower profiles show the observed Bouguer anomaly (thick grey line) and calculated Bouguer anomaly profiles (thin solid line) for $0 < T_e < 180$. The 'best fit' profile is highlighted as a dashed line. The inset shows a plot of the RMS difference between observed and calculated gravity for different T_e. b) Central profile, profiles as in a). c) Eastern profile, profiles as in a).

ilar results. We found, however, using synthetic tests that a finite difference method which takes into account the contribution of the Bouguer anomaly of both the top and base of the flexed crust, gives more realistic solutions for the flexed surfaces and a better defined RMS minima than does the method of McKenzie and Fairhead [2] (Fig. A2).

We therefore follow previous studies [7,27] and explicitly take into account the known surface topographic loads and the multiple density interfaces that arise from flexure. The parameters used were as defined in Table 1. The values of Young's modulus and Poisson ratio are widely used in continental flexural studies. The densities of load and infill vary, but as has been shown they have a relatively small impact on the recovered T_e [33].

The discussion thus far has been in terms of surface, rather than sub-surface loads. Sub-surface loads due, for example, to intra-crustal thrusts, obducted 'blocks', and dense down going slabs, have been invoked to explain the Bouguer gravity anomaly 'couple' at some orogenic belts (e.g., Appalachians—[7], Apennines—[34], Taiwan—[35]). However, such a 'couple' is not observed in the India–Eurasia collisional system [7,6,36,14]. We therefore conclude that sub-surface loads do not significantly contribute to the gravity field in this region.

Fig. 1 compares the observed Bouguer gravity anomaly along 3 profiles of the eastern, central and western Himalaya foreland to calculated profiles. The observed profiles were constructed from a grid of Bouguer gravity and topography data compiled by GETECH (UK) as part of their South-East Asia Gravity Project (SEAGP). The Bouguer anomaly data is terrain corrected out to 167 km and has had a long wavelength satellite-derived gravity field complete to degree and order 20 removed from it [37]. We chose this field because it is dominated by the Indian Ocean gravity 'low' which most workers attribute to deep processes in the sub-lithospheric mantle. The calculated profiles assume that surface topographic loads in the Himalayas have flexed one end of a broken elastic plate. By calculating the RMS difference between observed and calculated Bouguer anomalies (Fig. 2), we estimate a best position of the plate break with respect to the mountain front and T_e for each of the profiles. Fig. 1a–c shows the topography and gravity anomalies stacked with respect the best plate break. The central profile (Fig. 1b) reveals a best fit T_e of 70 km. Fig. 2 shows the technique also recovers the position of the plate break. Fig. 2 highlights the fact that no value of $T_e < 70$ km can account for the central profile, irrespective the plate break location. The eastern and western profiles (Fig. 1a and c) show significantly lower values, however, of 50 and 30 km, respectively.

The results in Fig. 1 are in accord with previous studies. In particular, they agree ith the high T_e values reported by Lyon-Caen and Molnar [6] and Karner and Watts [7] for the central Himalaya foreland. They also confirm the earlier suggestion of Lyon-Caen and Mol-

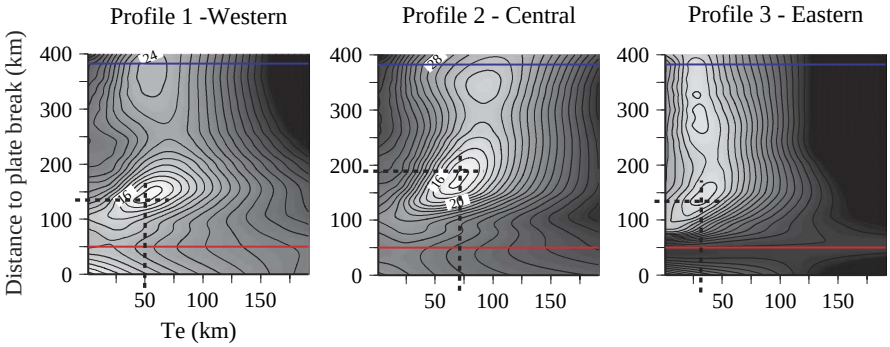

Fig. 2. Plots of RMS error between observed and calculated Bouguer gravity anomalies for the western, central and eastern profiles (Fig. 1). The thick dashed lines show the 'best fit' recovered values for the T_e and distance to the plate break from the mountain front. The western and central profiles show a well-defined minima and, hence, both the T_e and plate break are recovered along these profiles. The Eastern profile does not show a single well-defined minima, which we attribute to the fact that at low T_e the flexure is relatively insensitive to the width of the load.

nar [33] that T_e decreases to the west and east. Although our values in the west disagree with those recovered by Caporali [36] based on end-conditioning loads, they agree well with those of Cattin et al. [14] in the east who used actual topographic loads.

4. 2-dimensional modelling

In order to verify the T_e structure inferred from individual profiles, we have developed a technique to recover spatial variations in rigidity directly from grids of topography and Bouguer gravity anomaly data. The technique assumes that a) the topography represents the only load on the lithosphere that deforms by elastic plate flexure, b) the flexure involves the deformation of the top and bottom of the crust, and c)the principal contribution to the Bouguer anomaly is from the gravity effect of the two interfaces that bound the flexed crust.

The technique incorporates a 2-dimensional finite difference method to calculate the flexure and a Fast Fourier Transform method to calculate the gravity anomaly. The finite difference method has previously been used by van Wees and Cloetingh [30] and is as described in the Appendix of Stewart and Watts [27]. The main difference is that all boundaries of the plate are assumed to have free-edges. Wyer [38] has shown that this assumption yields a flexure that agrees to within 1% of the analytical solution for a simple disc-shape load on an elastic plate with uniform T_e [39]. The gravity anomaly modelling method is based on Parker [40] and includes higher order terms up to 4.

The modelling process has two parts. The first part follows [25] and uses grids of Bouguer gravity anomaly and topography data to recover an initial T_e structure. For each structure, the flexure below an input topographic load and its associated Bouguer gravity anomaly are calculated. The modelled Bouguer anomaly is then compared to observations in a ‘5 by 5 ’point window and the RMS difference between them calculated. The RMS difference is assigned to the window centre and the window is shifted by 1 point. The process is repeated thereby generating a RMS difference map for each constant T_e structure. The T_e is selected which gives the lowest RMS difference at each point in the grid. Finally, the resulting T_e structure is smoothed using a Gaussian filter since such filters avoid side lobes and reduce rapid variations in the rigidity which could cause instability in the finite difference modelling.

The second part is an iterative one which refines the smoothed T_e structure. The flexure and Bouguer gravity anomalies associated with the ‘initial variable T_e structure’ are calculated. Also calculated are the effects of shifting the entire T_e structure by $-4,-2,+2$ and $+4$ km. RMS difference maps are created for each of these 5 variable T_e structures. The shift in T_e at each point which gives the lowest difference is applied to the ‘initial variable T_e structure’. This new variable T_e structure is then smoothed with a Gaussian filter. This structure is passed back to the start and the process repeated until the model is deemed to be stable. Finally, an assessment of the stability of the model is made based on how much T_e has changed over the last 5 iterations.

5. Synthetic tests

We have tested the iterative method by first constructing a synthetic gravity anomaly and topography data set based on a known T_e structure and then using it to recover T_e. The modelled flexure assumes a fractal load that is superimposed on a 2-dimensional elastic plate with a spatially varying rigidity [41,24]. The topography is calculated by addition of the load to its associated flexure. The Bouguer gravity anomaly was calculated from the flexure, assuming a single interface at the crust mantle boundary (i.e., load density = crust density).

Fig. 3 shows how well the iterative method recovers T_e for a range of noise levels in the synthetic data and ratio, F, of surface to sub-surface loading [42]. The figure shows that in the absence of noise (i.e 0%) and sub-surface loading (i.e., $F=0$) that the shape of the input T_e structure is recovered well. The maximum value of T_e recovered was 58.2 km compared to 50.0 km that was input. This overestimate is probably due to the fact that the modelled topography includes flexural bulges. The bulges are treated as loads by the iterative technique and therefore should be removed from the input topography. Unfortunately, this is difficult to do without a priori knowledge of the T_e structure.

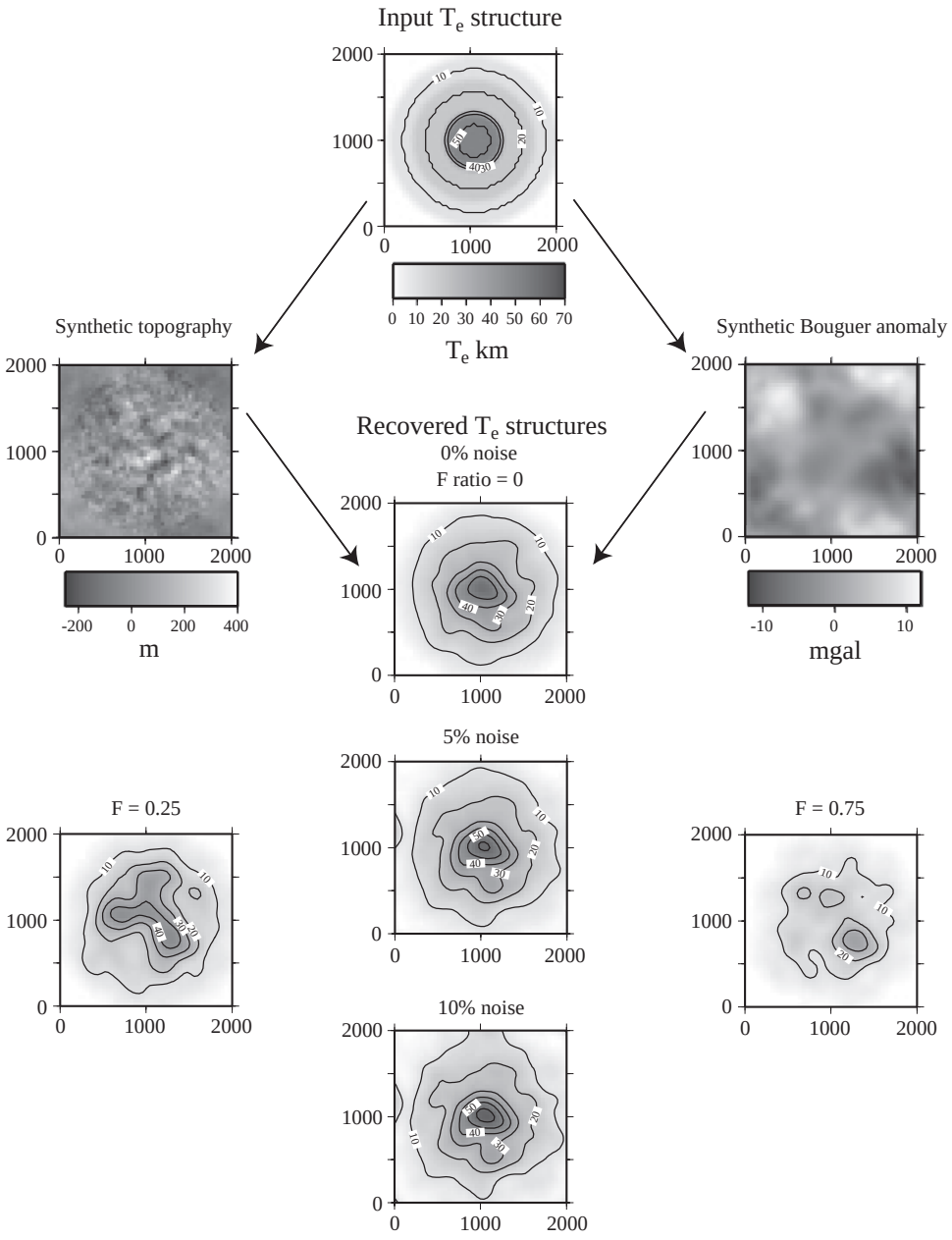

Fig. 3. Synthetic tests of the 2-dimensional iterative method. The upper 3 panels show the synthetic topography and gravity generated by loading an elastic plate with the T_e structure shown. The central 3 panels show with the recovered T_e structure with surface loading only (i.e., $F=0$) and increasing amounts of noise. The lower left and right panels show with the recovered T_e structures with $F=0.25$ and $F=0.75$, no noise, and with sub-surface loading occurring at the base of the crust. The recovered T_e structures were all smoothed using a 400 km Gaussian filter.

The recovery of T_e is not as good when either the noise levels or F are increased. The sensitivity to noise was evaluated by adding 5% and 10% random Gaussian noise to the synthetic Bouguer gravity data for $F=0$. Although the shape of the input T_e structure is retained, the absolute values of the recovered T_e

increase, particularly over the highest T_e areas. This increase, however, is relatively small (maximum T_e with 10% noise is 64 km compared to 50 km). The sensitivity to F was considered for values of F of 0.25 and 0.75. Again, the shape of the input T_e structure is retained. However, as the amount of sub-surface loading increases ($F=1$ corresponds to an equal amount of surface and sub-surface loading), the maximum values recovered decreases. This is because a high T_e sub-surface loads have small topographic expressions relative to the mantle topography, which generates the Bouguer gravity anomaly. When the T_e is low, however, (as it is towards the edges of the model) then the recovery is good.

These tests with a synthetic gravity and topography data set show that the iterative method recovers an input T_e structure well. The best recovery is for low noise levels and small amounts of sub-surface loading. This is true even in the case of subdued topography, the maximum used here being in the range ± 400 m.

Incorporation of mechanical discontinuities such as breaks into an elastic plate model is a difficult problem, which is beyond the scope of this paper. We have shown, however, in tests with synthetic data, using both 1-dimensional and 2-dimensional models, that a T_e that decreases to 0 km over a short distance is, in fact, a good proxy for a plate break.

6. Results

We have applied the iterative method to determine the T_e structure of the India-Eurasia collisional system. Fig. 4e shows the recovered T_e together with the observed (Fig. 4a) and calculated (Fig. 4b) Bouguer gravity anomaly. The figure shows that T_e varies widely across the region, with recovered values ranging from 125 km in the Himalayan foreland to nearly 0 km in the Tibetan plateau. There is an excellent agreement between the observed Bouguer anomaly and the calculated anomaly based on the T_e structure.

A useful way to evaluate the role of flexure is by consideration of the isostatic gravity anomaly. We first consider the Airy isostatic anomaly which is defined as the difference between the observed Bouguer gravity anomaly and the gravity effect of the Airy-type compensation. This scheme of compensation considers the topography as a load on the surface of an elastic plate with a T_e of 0 km. If all the topography in a region is locally compensated, then the Airy isostatic anomaly should be nearly zero. Alternatively, if the topography is flexurally compensated then a distinctive pattern of Airy isostatic anomalies should be seen.

Fig. 4c shows that Airy isostatic anomalies are generally subdued, especially over the Indian peninsula, central Tibet, and Burma and south-west China. The most striking feature of the figure is the positive–negative ‘couple’ that correlates with the Himalayan mountain belt and its flanking foreland basin. The negative part of the ‘couple’ occurs over the foreland basin, suggesting that the Moho is deeper here than is predicted by Airy. The positive occurs over the Himalayan mountains, suggesting that the Moho is shallower here than is predicted by Airy. We attribute the ‘couple’ to flexure of the Indian lithosphere by the topographic loads of southern Tibet and the Himalaya. There is evidence from the amplitude of the ‘couple’ that the role of flexure decreases from the central part of the mountain front to the west and east. Northern and eastern Tibet also show a ‘couple’, although it is of smaller amplitude. Interestingly, the south-eastern corner of the plateau lacks a ‘couple’, suggesting his region is in Airy isostatic compensation.

We next consider the flexural isostatic anomaly which is defined as the difference between the observed Bouguer gravity anomaly and the gravity effect of the compensation based on the recovered T_e structure in (Fig. 4b). The flexural isostatic anomaly (Fig. 4d) is generally of smaller amplitude than the Airy isostatic anomaly (Fig. 4c), which is indicative of a regional rather than local-type compensation. The positive–negative ‘couple’ so visible in the Airy isostatic anomaly map, for example, is now absent.

The role of flexure is particularly well illustrated in power spectra plots of the different isostatic anomalies. Fig. 4f shows, for example, power spectra plots for a central rectangular region of the study area (dashed line, Fig. 4c). The plots show that the recovered T_e structure significantly reduces the power of the isostatic anomaly compared to Airy (i.e., $T_e=0$ km) and uniform T_e values of 40 and 100 km. These considerations indicate to us that a spatially varying T_e describes well the state of isostasy in the region.

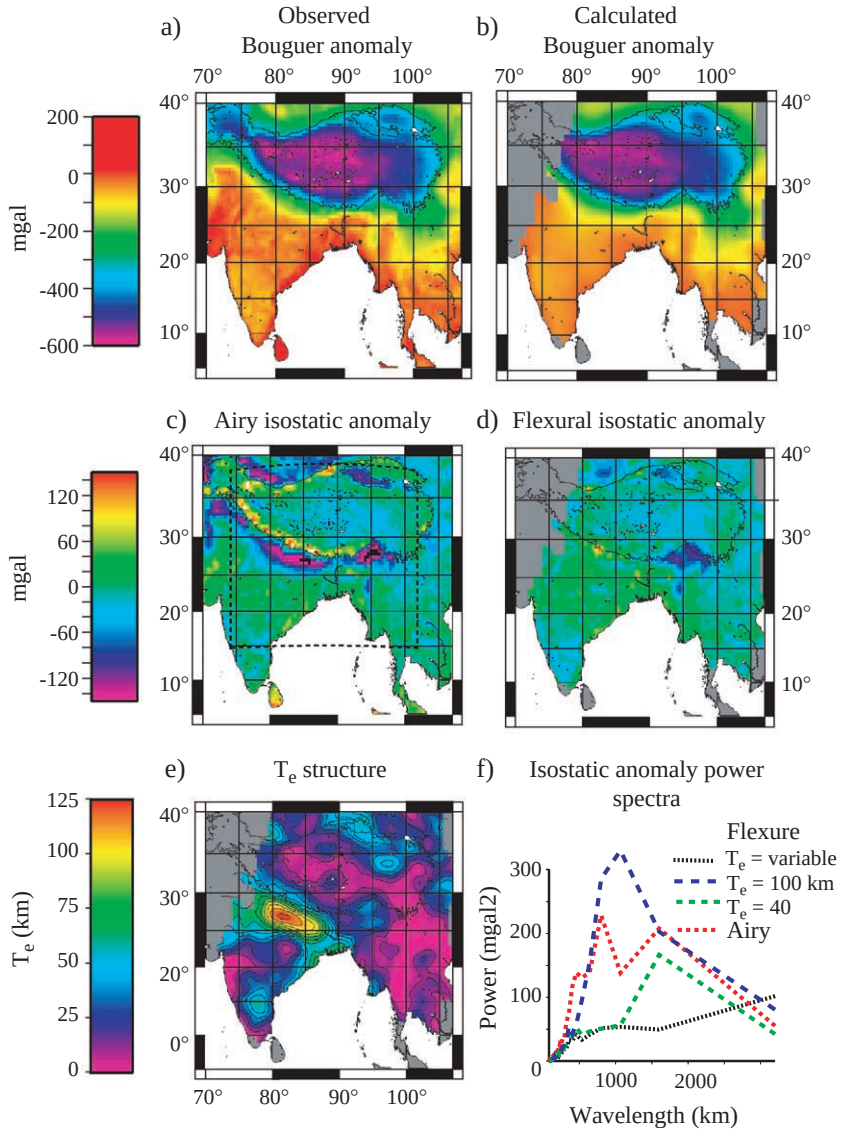

Fig. 4. Bouguer gravity anomalies, Isostatic anomalies, and the recovered structure T_e in the India–Eurasia collisional system. a) Observed Bouguer gravity anomaly from the GETECH [69] data base. The Bouguer gravity data was provided as 2.5 × 2.5 min 'smoothed' values which we have been gridded using GMT (surface) with a tension, T, of 0.25 and a grid spacing of 5 min. b) Calculated Bouguer gravity anomaly (stabilized regions only) after 30 iterations of the model. c) Airy isostatic gravity anomaly, calculated by subtracting the gravity effect of the Airy (i.e., T_e=0 km) compensation from the Bouguer anomaly. Dashed box outlines the analysis region for the power spectral plots in Fig. 4f. d) Flexural isostatic gravity anomaly, calculated by subtracting the gravity effect of the flexural compensation from the Bouguer anomaly. e) Recovered T_e structure obtained after 30 iterations. Contour interval=10 km. Output T_e structures were smoothed using a 350 km Gaussian filter. f) Power spectra of the Airy, T_e=40 km, T_e=100 km and variable T_e flexural isostatic anomalies. The isostatic anomaly based on the variable T_e spectra shows the least power. Parameters as in Table 1.

The main departures in the flexural isostatic anomaly in Fig. 4d are limited to the Qaidam Basin, north of the Tibetan Plateau, and to the eastern syntaxis of the Himalayas. The Qaidam Basin is underlain by 7–10 km [43] of alluvial plain sediments and it is likely that these sediments account for the discrepancy. The

origin of the discrepancy at the eastern syntaxis, however, is not as clear. The region, which shows high uplift rates (3 to 5 mm/yr [44]), is associated with oblique convergence and strike-slip faults and we speculate that the discrepancy is in some way the consequence of this tectonic complexity.

The reliability of the T_e structure in Fig. 4e can be accessed by consideration of its stability and sensitivity. The stability, which we define as the change in T_e structure over successive iterations, is shown in Fig. 5a. The white areas in the figure show regions of convergence where little further change in T_e occurs with subsequent iteration. The black and white dashed line in Fig. 5a shows the regions where the model appears to be stable. These include most of peninsula India, the Tibetan Plateau, and southwest China and Burma. The sensitivity, which we define as the deviation in the Bouguer anomaly due to small shifts of the T_e structure, is shown in Fig. 5b. The figure shows high sensitivity around the edges of the Tibetan Plateau, suggesting that T_e is well resolved in these regions. Although the sensitivity is low over peninsula India, it is non-zero and therefore some estimate of T_e can be recovered even in this topographically subdued region.

A final test of the iterative method is to visually compare observed and calculated gravity anomalies along selected profiles of the region. We selected 4 profiles, three of which coincide with the eastern, central and western profiles shown in Fig. 1. The other profile (dashed line on the map in Fig. 1) crosses the southeast margin of the Tibetan plateau.

Fig. 6a–c show the Bouguer gravity anomaly based on the spatially varying T_e structure fits the observed data well along the western, central and eastern profiles. The calculated profiles explain the amplitude and wavelength of the observed profiles in the region immediately beneath the load and in flanking areas. On the central profile, no uniform T_e fully explains the observed Bouguer gravity anomaly. A uniform T_e of 100 km accounts for the data in the foreland region, but fails to explain the anomaly immediately beneath the load. A uniform T_e of 40 km accounts for the data beneath the load, but not in the foreland region. On the western and eastern profiles, however, a uniform T_e of 40 km appears to explain the gravity anomaly data both beneath the load and flanking regions. We attribute this to the fact that there is less variation in T_e along these profiles, as seen in the recovered T_e values which average ~40 km along much of their length.

In contrast to the western, central and eastern profiles, the southeast margin of Tibet profile shows a relatively constant, low, T_e structure Fig. 6d. The

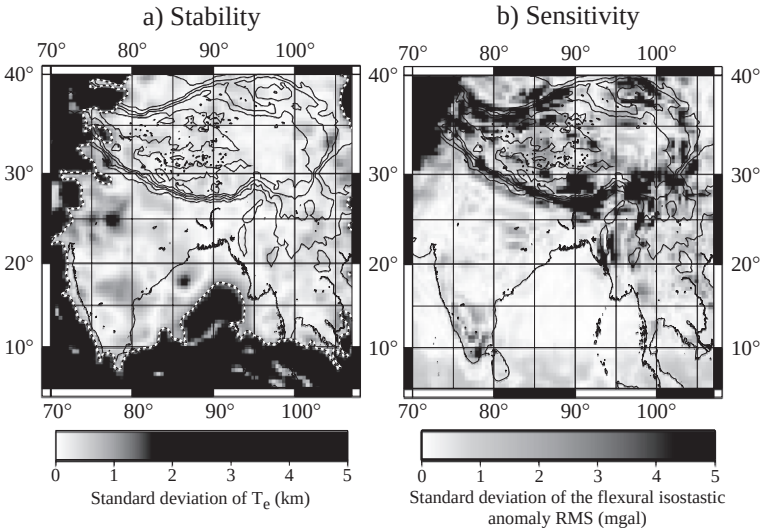

Fig. 5. Reliability of the iterative 2-dimensional technique as expressed by stability and sensitivity. a) Stability as revealed by the standard deviation of the T_e over the final 5 iterations. The dashed line delimits the area of high stability. b) Sensitivity as revealed by the standard deviation of the RMS difference between observed and calculated gravity anomalies based on small shifts in the final T_e structure.

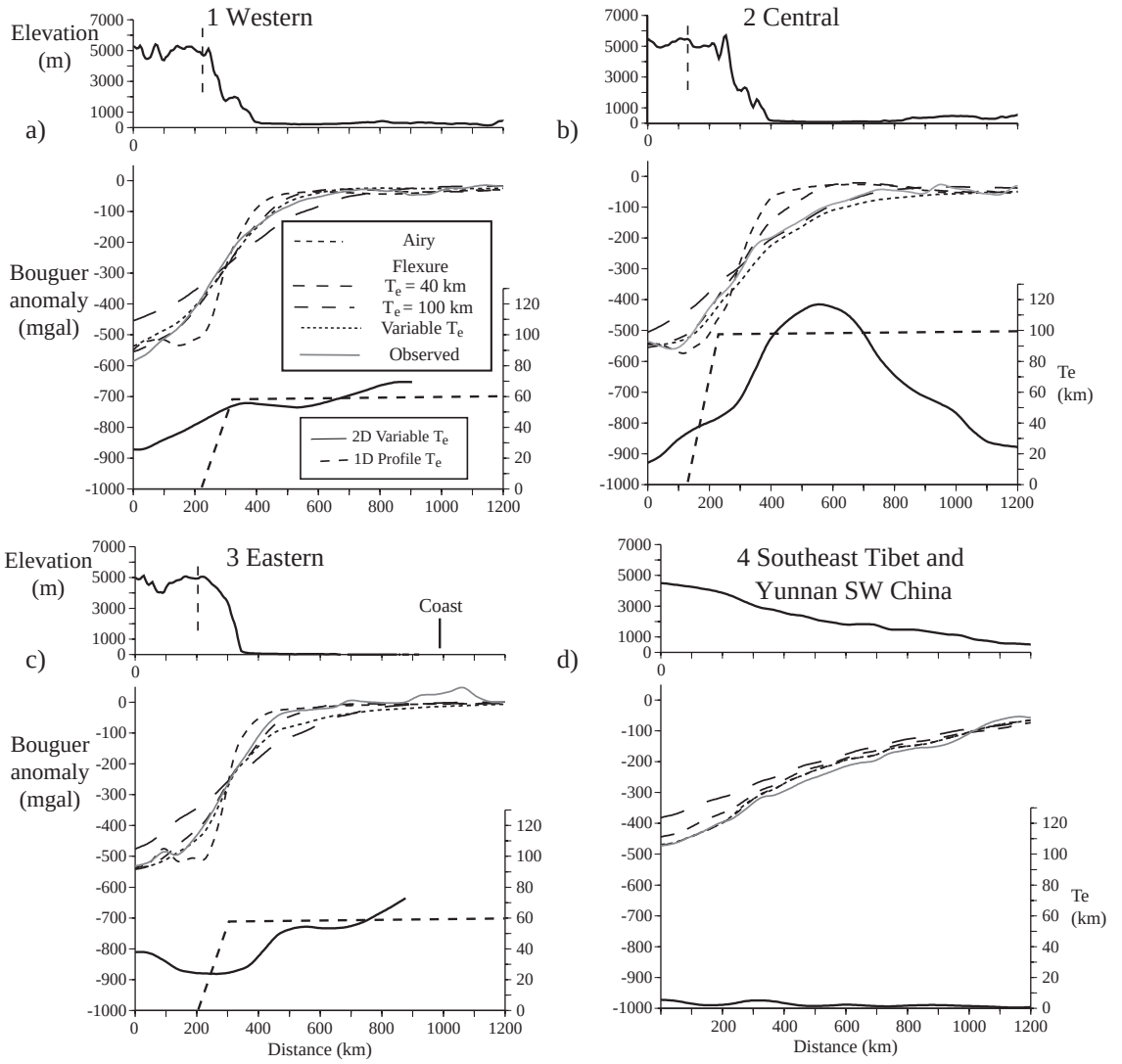

Fig. 6. Comparison of observed and calculated gravity anomalies on profiles of the Himalaya foreland and southern margin of the Tibetan Plateau (see Fig. 1 for location). The calculated anomalies are based on spatially varying T_e and uniform T_e structures of 0, 40 and 100 km. Also shown is the topography and recovered spatially varying T_e and the best fitting T_e structure from the 1D profile methods shown in Fig. 1. a) Western profile of the Himalaya foreland. b) Central profile. c) Eastern profile. d) Southeast margin of the Tibetan plateau and southwest China (Yunnan).

Airy model (i.e., T_e=0 km) and the variable T_e structure yield virtually identical calculated Bouguer anomalies. This could be a consequence of the long wavelength of the topography which makes a region appear weak, irrespective of its actual strength (e.g., [1]). We believe, however, that T_e is low, as seen by the inability of a high T_e (40, 100 km) to adequately recover details of the observed profile, such as the small amplitude anomalies between 500 and 900 km.

7. Discussion

7.1. Comparison with previous T_e estimates

There have been a number of previous estimates of T_e in the Himalayan foreland region. In the central region our estimates of 70 km based on forward modelling and 125 km based on the iterative method (Figs. 1 and 7) agree with previous results [6,7]. We

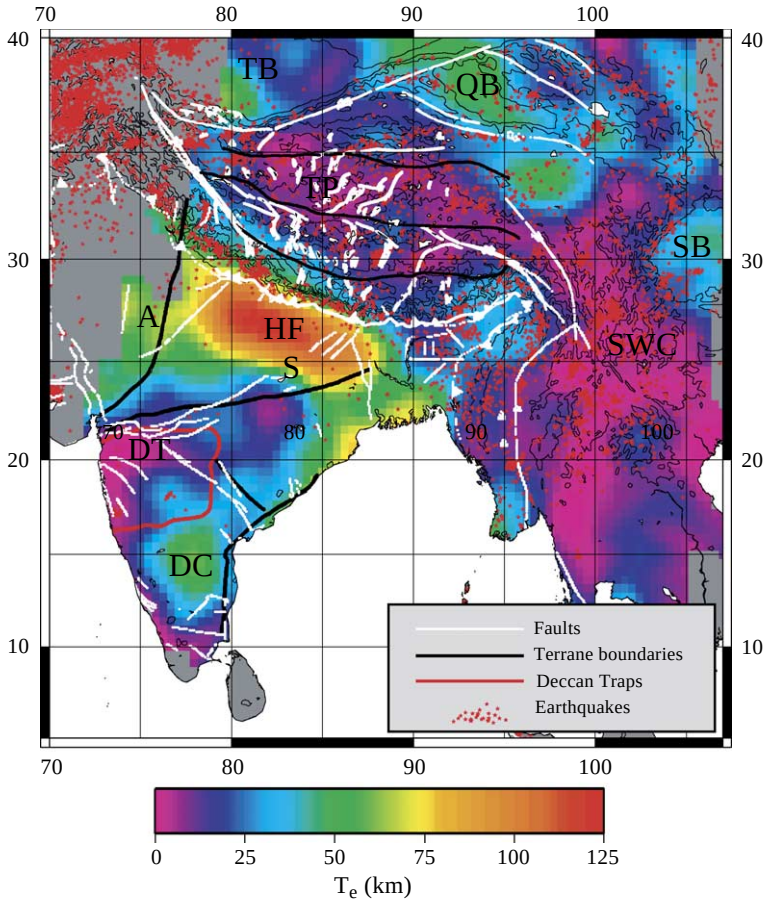

Fig. 7. The T_e structure of the India–Eurasia collisional zone. Thin black lines show topographic contours at 500 m intervals. Thick black lines show with the terrane boundaries from various authors ([70] Tibetan plateau and [52,71,72] over Peninsula India). Thick white T_e lines show faults from Yin [70] and Searle (pers.com.) over the Tibetan plateau and Dasgupta et al. [73] over peninsula India. Red stars show earthquakes (1979 to present), less than 50 km depth and all magnitudes [74]. HF=Himalayan foreland, DT=Deccan Traps, DC=Dharwar Craton, QB=Qaidam Basin, SB=Sichuan Block, TP=Central Tibetan plateau, SWC=Southwest China (Yunnan), A=Aravalli fold belt, S=Satpura Mobile Belt.

agree therefore with the conclusions of McKenzie and Fairhead [2] and Jackson et al. [45] that the northern Indian shield and Himalayan foreland is unusually strong. We do not agree, however, with the low (24 to 42 km) T_e values that these authors recover. As Fig. 1 clearly shows, T_e values this low cannot account for the amplitude and wavelength of the observed Bouguer gravity anomaly in the central foreland region. The iterative method reveals that T_e decreases from the central foreland to the east and west. In the east, our values of $30<T_e<60$ km agree with the result of Cattin et al. [14] who recovered a T_e of 50 km in this area.

Over the Tibetan plateau, we recover a variable T_e in the range 5–35 km with the lowest estimate corresponding to the central part of the plateau. Rajesh and Mishra [17] recover a T_e of 50 km using spectral methods across the entire region, which maybe the result of their averaging of the T_e structure of both the foreland and the plateau. Rajesh et al. [18] used similar methods to recover a T_e of 35 km across the Himalayan foreland, 20 km in the central plateau region, and 25 km for the northern margin of the Tibetan plateau and the Tarim and Qaidam basins. The results in the central area are close to those recovered in this study, but the values recovered to

the north and south, although higher than in the central region, are not as high as we derive. We attribute this to their use of relatively narrow analysis windows (500 km wide) which prevents the recovery of high T_e [24,46].

Braitenberg et al. [47] recover a spatially varying T_e structure across the Tibetan Plateau which agrees well with our results, particularly over the Qaidam basin area where we recover values of 50–60 km while [47] recovers 60–80 km. Jiang et al. [48] concluded that T_e along the northern margin of the plateau was in the region of 40–45 km assuming a broken plate along the Altyn Tagh and Kunlun faults. This in accord with our results. Yang and Liu [49] recover values from 60 to >100 km over the central Tarim basin. This also agrees with our results of ~50 km in the west of the basin. At the southern margin of the basin, however, these workers recover lower T_e values (24 km) which they suggest correlate with intensive and localised faulting. Finally, to the east of the plateau, Yong et al. [50] have recovered T_e values of 43–54 km for a Triassic foreland basin [50], which are somewhat higher than those recovered in this study (20–45 km).

The iterative method reveals that the Indian peninsula, south of the Himalayan foreland, has a highly variable T_e structure. In the region of the Deccan Traps, we recover T_e values of <5 km on the coast, rising to approximately 30 km to the west across the shield. These values are significantly less than those estimated by Watts and Cox [51] on the basis of the width of the lavas, but agree with the value of 8 km recovered from spectral analysis along profiles [15]. Stephen et al. [16] also used spectral methods to recover T_e values across the southern Indian peninsula (Fig. 7, areas DT and DC). They obtained relatively uniform T_e values of 11–15 km which concur with our results over the Deccan Traps, but disagrees over the Dharwar craton where we have recovered values >65 km. This may be because of a 'cap' on the recovered T_e due to the window size used [24].

Recently, Rajesh and Mishra [19] determined the transitional Bouguer coherence wavelength in overlapping windows across peninsula India. The pattern of rigidity variation implied is very similar to the T_e structure recovered in this paper. However, the T_e values recovered (18–26 km in Northern India and 12–16 km in Southern India) are significantly lower than our values. We attribute this discrepancy to the fact that the T_e recovered by these authors are lower bounds, as indeed their RMS plots of the difference between observed and calculated Bouguer coherence suggest [19].

7.2. T_e and terrane structure

We compare in Fig. 7 the T_e structure of the India–Eurasia collisional system to the main terrane boundaries, faults, and earthquakes.

Over peninsula India, there is a general correlation between T_e terrane boundaries, faulting, and earthquakes. This is most clearly seen to the south of the Himalayan foreland where the region of high T_e is truncated by a fault which correlates with a suture zone (the Satpura Mobile Belt [52]). This and other terrane boundaries separate Archean–Proterozoic 'blocks' which appear to be more rigid and less prone to faulting than the intervening sutures. The terranes sutured together between 1600 and 500 Ma [52]. This suggests that suture zones are weak and have remained so over long periods of time. Evidence that old suture zones are areas of low rigidity also comes from spectral studies of other continents. Simons [53] showed, for example, that in the Australian continent suture zones are weak. We attribute his to the fact that old suture zones tend to be the sites of intra-cratonic fault localisation [54].

The terranes of the Tibetan plateau show a less obvious correlation with the T_e structure. There is a suggestion, however, that the southern most suture (the Zangpo suture) marks the limit of the high (>40 km) T_e zone which extends north from the Himalayan foreland. This is in accord with the results of the INDEPTH project [55] which show that north of the Zangpo suture the middle crust is partially molten. Seismic reflection profile data shows highly reflective 'bright spots' which are interpreted as fluid (probably magma) [56] at depths of 15–18 km beneath the central plateau. The presence of magma suggests that the crust below these depths is close to melting and, hence, these regions would be expected to be weak. This is likely to be particularly true for the central and northern parts of the Tibetan plateau that are not underlain by Indian continental shield material.

The northern and eastern edges of the Tibetan plateau are bordered by the Tarim, Qaidam and Sichuan basins. Although these regions are not delimited by

terrane boundaries in Fig. 7, they are believed to be underlain by fragments of old cratonic 'blocks'. The Qaidam basin, for example, is underlain by Palaeozoic crust [57] and the Sichuan basin by Proterozoic basement [58]. These 'blocks' correlate with lower levels of seismicity and apparently are of higher T_e than surrounding regions.

7.3. T_e and crust and mantle strength

The T_e values recovered in this study are, in places, high and clearly exceed the seismogenic layer thickness, T_s [8]. This is best seen in the central Himalayan foreland where T_e is >70 km and T_s is ~40–45 km (Fig. 7). The T_e values greatly exceed the crustal thickness (40–44 km) [59] which implies that the sub-crustal mantle must, in places, be rigid enough to significantly contribute to the long-term integrated strength of the lithosphere.

The fact that the sub-crust mantle can be involved in the support of long-term loads, is not surprising given that in oceanic areas, away from a mid-ocean ridge, T_e greatly exceeds the crustal thickness. As shown by Watts [1] oceanic T_e values lie within the depth to the 300–600 °C isotherms as defined by a cooling plate model. Therefore, a significant portion of the sub-oceanic mantle is strong down to depths of up to ~50 km.

Seismic tomographic data shows that the mantle below parts of the continents has a significantly higher shear wave velocity at 120 km depth than has the oceans [60]. If the mantle is cooler below the continents than the oceans, as these data suggest, then it is likely that it is rigid to a greater depth. Therefore continents, where they have cold mantle roots, would be expected to be stronger than the oceans.

Further lines of evidence that the continental mantle has some rigidity over long periods of time comes from direct samples and thermal modelling. McKenzie [61], for example, showed that the geotherm of the Archean Kaapvaal craton in South Africa could be modelled as a plate with a mechanical boundary layer thickness of 165 km and a interior potential temperature of 1280 °C. This thickness compares to ~100 km for the equivalent layer in the oceans. Extrapolating the geotherm shown in [61] gives a depth to the 600 °C isotherm of 75–80 km. At these temperatures, by analogy with the oceans, the mantle, if it is dry, will be rigid enough to provide a significant contribution to the observed T_e. McKenzie [61] also presents data from sheared peridotite nodules which originate from depths greater than about 160 km, geochemical studies of which show them to be part of the convecting mantle. Nodules shallower than 160 km are not sheared, suggesting that this part of the mantle is behaving rigidly when stressed by convection.

The great depth to the convecting mantle in continental regions is in accord with the results of Simons [53] based on spectral and tomographic studies in the Australian shield. They showed that a correlation exists between the isostatic (as defined by the directional Bouguer coherence) and seismic anisotropy down to a depth of almost 200 km and therefore that the lithosphere is apparently rigid to these depths. At greater depths, the correlation breaks down and while the mantle may have a preferred orientation on short seismic time-scales it appears weak on the long time-scales associated with flexural isostasy [53].

If the Kaapvaal and Australian cratons are typical of Archean shield areas, then other shields, such as the Himalayan foreland, should also be rigid we believe to great (150–200 km) depths. The high T_e recovered in parts of the Indian peninsula is therefore a manifestation of this rigidity. We cannot, however, determine the actual thickness of the rigid layer from isostatic studies because, as a number of authors have shown (e.g., [62]), T_e is not the actual depth to which materials behave elastically, but reflects the integrated strength of the lithosphere.

7.4. T_e and ductile crustal deformation

We have shown that the elevated regions of the south-eastern margin of Tibet and Yunnan are associated with low values of T_e suggesting that they may be locally compensated (SWC—Fig. 7). The region therefore differs from, other parts of the margin (e.g., the Himalayan foreland) which appear to be regionally compensated by a strong under thrusting lithospheric plate. If the south- eastern margin of the plateau, east of the eastern syntaxis, is not associated with under thrusting of a strong plate, then the question arises as to why it is elevated? One possibility is some form of lower crustal flow [63–65]. According to this model, low viscosity lower crustal material flows out from beneath the Tibetan plateau and 'inflates' south-west China.

Previous authors (e.g., [66]) have argued that the Tibetan plateau can be modelled as a thin viscous sheet which is deformed by a rigid 'indenter' to the south. This model was able to incorporate higher viscosity (more rigid) blocks. These deformed much less than the surrounding material and generated regions of low relief which were suggested to be analogous to the Tarim basin to the north of the Himalayas.

Royden et al. [63] pointed out that a viscous sheet, however, is unrealistic since such models do not incorporate a vertical stratified rheology. They therefore proposed instead a model in which the upper crust and mantle are effectively decoupled by a low-viscosity lower crust during compressional deformation.

Clark and Royden [64] show that there are two 'end-members' for the topographic gradient of the Tibetan plateau margin; steep (e.g., southern Himalaya, Tarim and Sichuan basins) and shallow (e.g., Yunnan, south-western China). They model these end member cases in terms of a channelised viscous flow in the lower crust. In the steep case, the channel contains high viscosity material and a steep topographic gradient develops. In the shallow case, a low viscosity channel inflates the crust, giving rise to a shallow gradient. They showed that the Tibetan plateau was surrounded by a number of rigid 'blocks', which included the Tarim, Qiadam, and Sichuan basins and the Indian shield. The lower crust, they argued, would preferentially flow around these 'blocks' and in the process generate the shallow topographic gradients seen at the present day in south-west China.

The high T_e areas mapped in this study supports the view that deformation in the Tibetan plateau and surroundings has involved 'blocks' that have remained rigid for long periods of time. However, the mechanism of crustal thickening across the region is more complex, we believe, than has been previously suggested. We know that in the regions of steep topographic gradients, surface loads are compensated, at least in part, regionally not locally as has been assumed by previous authors [66,63,64]. Moreover, it is hard to reconcile the underthrusting of the rigid Indian lithosphere beneath the Tibetan plateau [55] with viscous injection and flow of the lower most crust. Searle et al. [67], for example, showed that in the Mt Everest region mid-crustal material has plastically extruded to the surface from depths of 12–18 km and laterally from approximately 200 km to the north. This suggests that the topography of the high Himalaya is generated, at least in part, by viscous flow of mid-crustal material that is over-riding the strong Indian plate, rather than by inflation of the lower crust [64].

We support, however, the arguments of Clark and Royden [64] for lower crustal flow in the shallow topographic gradient areas of south-west China (Yunnan). Wang [68] has shown, from a GPS-derived velocity field, that central Tibet is, on a large scale, deforming continuously and that material is being extruded from the Tibetan plateau to the south east. This we believe represents movement of weak surface crustal material deforming and moving to the south east with the lower crust beneath it. The pattern of deformation is consistent with he results of this study, which show a broad region of low T_e beneath the Tibetan plateau which appears to continue between high T_e regions and into south-west China (Yunnan). This region of low T_e may represent the isostatic signal of the weak, flowing, lower crust.

8. Conclusions

1. The iterative method is a non-spectral technique that successfully recovers a spatially varying T_e structure *directly* from observed topography and Bouguer gravity anomaly data.
2. Application of the method to the India–Eurasian collisional system reveals acomplex T_e structure with both high and low rigidity areas.
3. The Himalaya foreland is a high T_e region ($40 < T_e < 100$ km) which forms a rigid 'block' with well defined edges, as shown by localisation of faulting and deformation along its northern margin. Other rigid 'blocks' have been identified in the region of the Qaidam and Sichuan basins.
4. The Tibetan plateau is a low T_e region ($0 < T_e < 20$ km) which forms a weak zone that separates these rigid blocks. The weak region extends into south-west China (Yunnan) where T_e is also low.
5. Within cratonic regions there is evidence (e.g., Indian peninsula) that the rigid blocks are separated by weaker areas which correlate with ancient suture zones.
6. Tectonic styles in the India–Eurasian collisional system involve both rigid and non-rigid 'blocks'. Where high rigidity 'blocks' are present the style is

dominated by underthrusting of the more rigid 'block'. Where the collisional zone is not constrained by rigid 'blocks' the style appears to be dominated by lower crustal flow and continuous deformation.

Acknowledgements

We thank Mike Searle for his comments. This research was supported by a NERC advanced studentship NER/S/A/2002/10530 to TAJ and NERC grant NER/A/S/2000/00454 to ABW.

Appendix A

We used in the analysis of 1-dimensional profiles a finite difference method in which the flexure and Bouguer gravity anomaly associated with an arbitrary shaped surface topographic load is calculated and compared to observations. The method was tested by comparing it directly to the analytical solution of the Hetényi [31]. The Hetényi [31] solution was used to calculate the flexure and Bouguer gravity anomaly associated with a 5 km high, 200 km wide, rectangular 'driving' load, one edge of which is located on a discontinuous (i.e., broken) plate with T_e=90 km (Fig. A1a,b). We then used the finite difference method to calculate the flexure and Bouguer gravity anomaly for a range of values for the distance from the load edge to the plate break, x_{pb}, and T_e. The plate break was simulated by assuming T_e=0 at the plate break (x=0) and T_e=90 at $x \geq 100$ km. Fig. A1c shows a plot of the RMS difference between the calculated Bouguer gravity anomaly based on the Hetényi [31] solution and the finite difference method for different x_{pb} and T_e. The figure shows a well defined minima in the RMS a x_{pb}=200 km and T_e=90 km, demonstrating that the finite difference method recovers well both the distance from the edge of the load to the plate break and the elastic thickness.

The finite difference method of recovering T_e is similar to that used by previous workers (e.g., [27]), but differs from that of McKenzie and Fairhead [2]. These authors used a shape-fitting technique to estimate T_e directly from the free-air anomaly. Their method has the advantage that it does not require that either the load or plate break be specified a priori.

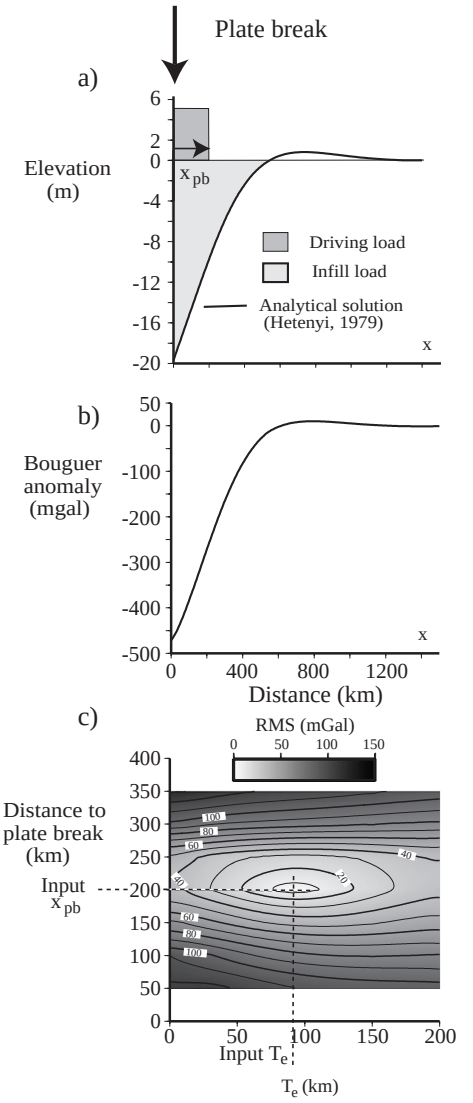

Fig. A1. Comparison of the analytical solution of Hetényi [31] for a discontinuous (i.e., broken) plate and the finite difference method. a) Analytical solution based on an input T_e=90 km and x_{pb}=200 km. The driving load is 5 km high and 200 km wide. The infill load is the material that infills the flexure. b) Calculated Bouguer gravity anomaly assuming two uniform density contrast interfaces, one at the top of the flexed crust and the other at the base. c) Plot of the RMS difference between the calculated Bouguer gravity anomaly in b) and a 'synthetic' anomaly calculated using a finite difference model with a range of values of T_e. The figure shows that the finite difference method recovers well both the input plate break and input T_e.

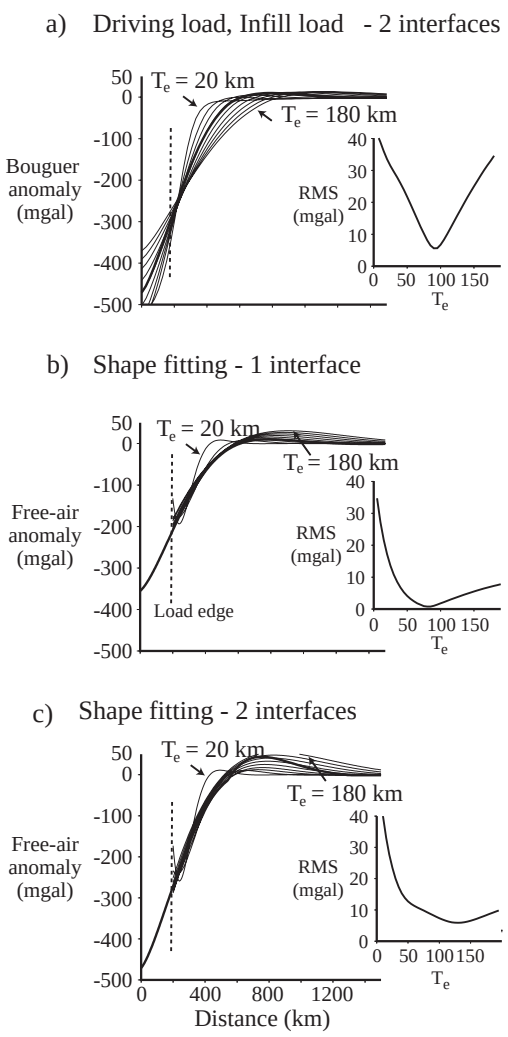

Fig. A2. Comparison of the RMS difference between calculated gravity anomalies based on the finite difference method, the shape fitting technique of McKenzie and Fairhead [2] and the analytical solution of Hetényi [31]. a) Calculated Bouguer gravity anomalies assuming two interfaces, between foreland basin sediments and crust, and crust and mantle, based on the finite difference method (thin lines). The thick line shows a 'synthetic' anomaly based on T_e=90 km, x_{pb}=200 km and the same two interfaces. The inset shows the RMS difference between the Bouguer anomaly associated with the finite difference model and the synthetic anomaly. b) Calculated gravity anomalies based on the shape-fitting technique [2] (thin lines) assuming a single uniform density contrast interface at the base of the flexed crust (i.e., Moho). The thick line shows the synthetic as defined in a) but for only the Moho interface. c) Calculated gravity anomalies, beyond the load edge, based on the shape fitting technique [2] (thin lines) compared to a multiple interface (free air) synthetic. The synthetic (thick line) assumes 3 interfaces, the Moho, the base of the foreland basin and the flexural bulge.

We found that although the two methods give generally similar results, the minima in the RMS difference between the gravity anomaly based on the finite difference and McKenzie and Fairhead [2] methods is better defined in the former than the latter. This is clearly seen in Fig. A2 which compares the two methods. The finite difference method (Fig. A2a) yields a well-defined RMS minima centred on T_e=90 km which is the T_e used in the analytical calculation [31]. The minima in the McKenzie and Fairhead [2] method, however, are broad and are centred on T_e=80 km when a single density interface at the Moho is used in the gravity anomaly calculation or T_e=125 km when interfaces at the top and base of the crust are assumed. We attribute these differences to the nature of the calculated flexure curves. In the finite difference method the shape of the flexure is determined by the height and width of the driving load. The flexural bulge, for example, migrates in a systematic way away from the load as T_e increases. In the McKenzie and Fairhead [2] method, however, the flexure shows departures. The bulge shows little or no migration as T_e increases. Moreover, a low T_e the flexure shallows towards the load edge. This is clearly not plausible if flexure is driven, as we believe, by downward-acting surface topographic loads.

References

[1] A.B. Watts, Isostasy and Flexure of the Lithosphere, Cambridge University Press, 2001, p. 458.
[2] D.P. McKenzie, D.J. Fairhead, Estimates of effective elastic thickness of the continental lithosphere from Bouguer and free-air gravity anomalies, J. Geophys. Res. 102 (1997) 27523–27552.
[3] T.D. Bechtel, D. Forsyth, V. Sharpton, R. Grieve, Variations in effective elastic thickness of the North American lithosphere, Nature 343 (1990) 636–638.
[4] M. Zuber, T. Bechtel, D. Forsyth, Effective elastic thickness of the lithosphere and mechanisms of isostatic compensation in Australia, J. Geophys. Res. 94 (1989) 9353–9367.
[5] N. Ussami, N.G. Sá, E. Cassola Molina, Gravity map of Brazil: 2. Regional and residual isostatic anomalies and their correlation with major tectonic provinces, J. Geophys. Res. 98 (1993) 2199–2208.
[6] H. Lyon-Caen, P. Molnar, Constraints on the structure of the Himalaya from an analysis of gravity anomalies and a flexural model of the lithosphere, J. Geophys. Res. 88 (1983) 8171–8191.

[7] G.D. Karner, A.B. Watts, Gravity anomalies and flexure of the lithosphere at mountain ranges, J. Geophys. Res. 20 (1983) 10449–10477.
[8] A. Maggi, J. Jackson, D. McKenzie, K. Priestley, Earthquake focal depths, effective elastic thickness, and the strength of the continental lithosphere, Geology 28 (2000) 495–498.
[9] J. Jackson, Strength of the continental lithosphere: time to abandon the jelly sandwich? GSA Today (2002) 4–10.
[10] J. Jackson, Faulting, flow and the strength of the continental lithosphere, Int. Geol. Rev. 44 (2002) 29–61.
[11] W.P. Chen, P. Molnar, Focal depths of intracontinental and intraplate earthquakes and their implications for the thermal and mechanical properties of the lithosphere, J. Geophys. Res. 88 (1983) 4183–4214.
[12] A.B. Watts, E.B. Burov, Lithospheric strength and its relationship to the elastic and seismogenic layer thickness, Earth Planet. Sci. Lett. 213 (2003) 113–131.
[13] M.R. Handy, J.P. Brun, Seismicity, structure and strength of the continental lithosphere, Earth Planet. Sci. Lett. 223 (2003) 427–441.
[14] R. Cattin, G. Martelet, P. Henry, J.P. Avouac, M. Diament, T.R. Shakya, Gravity anomalies, crustal structure and thermomechanical support of the Himalayas of Central Nepal, Geophys. J. Int. 147 (2001) 381–392.
[15] V.M. Tiwari, D.C. Mishra, Estimation of efective elastic thickness from gravity and topography data under the Deccan Volcanic Province, India, Earth Planet. Sci. Lett. 171 (1999) 289–299.
[16] J. Stephen, S.B. Singh, D.B. Yedekar, Elastic thickness and isostatic coherence anisotropy in the South Indian peninsular shield and its implications, Geophys. Res. Lett. 30 (2003) 1853–1856.
[17] R.S. Rajesh, D.C. Mishra, Admittance analysis and modelling of satellite gravity over Himalayas–Tibet and its seismogenic correlation, Curr. Sci. 84 (2003) 224–230.
[18] R.S. Rajesh, J. Stephen, D.C. Mishra, Isostatic response and anisotropy of the Eastern Himalayan–Tibetan Plateau: a reappraisal using multitaper spectral analysis, Geophys. Res. Lett. 30 (2003) 1060–1064.
[19] R.S. Rajesh, D.C. Mishra, Lithospheric thickness and mechanical strength of the Indian shield, Earth Planet. Sci. Lett. 225 (2004) 319–328.
[20] A.R. Lowry, R.B. Smith, Flexural rigidity of the basin and range—Colorado Plateau–Rocky Mountain transition from coherence analysis of gravity and topography, J. Geophys. Res. 99 (1994) 20123–20140.
[21] Y. Wang, J. Mareschal, Elastic thickness of the lithosphere in the central Canadian shield, Geophys. Res. Lett. 26 (1999) 3033–3036.
[22] P. Flück, R.D. Hyndman, C. Lowe, Effective elastic thickness T_e of the lithosphere in western Canada, J. Geophys. Res. 108 (2003), doi:10.1029/2002JB002201.
[23] R. Hartley, A.B. Watts, J.D. Fairhead, Isostasy of Africa, Earth Planet. Sci. Lett. 137 (1996) 1–18.
[24] M. Perez-Gussinye, A. Lowry, A. Watts, I. Velicogna, On the recovery of effective elastic thickness using spectral methods: examples from synthetic data and from the Fennoscandian shield, J. Geophys. Res. 109 (2004), doi:10.1029/2003JB002788.
[25] C. Braitenberg, J. Ebbing, H.J. Götze, Inverse modeling of elastic thickness by convolution method— the eastern Alps as a case example, Earth Planet. Sci. Lett. 202 (2002) 387–404.
[26] B.F. Windley, Framework for the geology and tectonics of the Himalayas, Karakoram and Tibet, and problems of their evolution, in: R.M. Shackleton, J.F. Dewey, B.F. Windley (Eds.), Tectonic Evolution the Himalayas and Tibet, vol. A326, 1988, pp. 3–16.
[27] J. Stewart, A.B. Watts, Gravity anomalies and spatial variations of flexural rigidity at mountain ranges, J. Geophys. Res. 102 (1997) 5327–5352.
[28] J. Bodine, Numerical Computation of Plate Flexure in Marine Geophysics, Technical Report, vol. 1, Lamont-Doherty Geological Observatory of Columbia University, New York, 1980, 153 pp.
[29] M.H.P. Bott, The use of rapid digital computing methods for direct gravity interpretation of sedimentary basins, Geophys. J. R. Astron. Soc 3 (1960) 63–67.
[30] J.D. van Wees, S. Cloetingh, A finite-difference technique to incorporate spatial variations in rigidity and planar faults into 3-D models for lithospheric flexure, Geophys. J. Int. 117 (1994) 179–195.
[31] M.I. Hetényi, Beams on Elastic Foundations: Theory with Applications in the Fields of Civil and Mechanical Engineering, University of Michigan Press, Ann Arbor, 1979, 255 pp.
[32] D.P. McKenzie, Estimating T_e in the presence of internal loads, J. Geophys. Res. 108 (2003), doi:10.1029/2002JB001766.
[33] H. Lyon-Caen, P. Molnar, Gravity anomalies, flexure of the Indian plate, and the structure, support and evolution of the Himalaya and Ganga basin, Tectonics 4 (1985) 513–538.
[34] L.H. Royden, G.D. Karner, Flexure of lithosphere beneath Apennine and Carpathian foredeep basins: evidence for an insufficient topographic load, Am. Assoc. Pet. Geol. Bull., Mem. 68 (1984) 704–712.
[35] A.T.-S. Lin, A.B. Watts, Origin of the West Taiwan basin by orogenic loading and flexure of a rifted continental margin, J. Geophys. Res. 107 (2002) 2185–2204.
[36] A. Caporali, Gravity anomalies and the flexure of the lithosphere in the Karakoram, Pakistan, J. Geophys. Res. 100 (1995) 15075–15085.
[37] R. Rapp, N. Pavlis, The development and analysis of geopotential coefficient models to spherical harmonic 360, J. Geophys. Res. 95 (1990) 21885–21991.
[38] P.P.A. Wyer, Gravity anomalies and segmentation of the eastern USA passive continental margin, Ph.D. thesis, Oxford University D.Phil, 263 pp. 2003.
[39] J.F. Brotchie, R. Silvester, On crustal flexure, J. Geophys. Res. 74 (1969) 5240–5252.
[40] R.L. Parker, The rapid calculation of potential anomalies, Geophys. J. R. Astron. Soc. 31 (1972) 447–455.
[41] C.J. Swain, J.F. Kirby, The effect of noise on estimates of the elastic thickness of the continental lithosphere by the coherence

method, Geophys. Res. Lett. 30 (2003), doi:10.1029/2003GL017070.
[42] D.W. Forsyth, Subsurface loading and estimate of flexural rigidity of continental lithosphere, J. Geophys. Res. 90 (1985) 12623–12632.
[43] A.W. Bally, I.M. Chou, R. Clayton, H.P. Eugster, S. Kidwell, L.D. Meckel, R.T. Ryder, A.B. Watts, A.A. Wilson, Notes on sedimentary basins in China: report of the American sedimentary basins delegation to the Peoples Republic of China, U.S. Geol. Surv. Open File Rep 108 (1990) 86–237.
[44] J. Burg, P. Davy, P. Nievergelt, F. Oberli, D. Seward, Z. Diao, M. Meir, Exhumation during crustal folding in the Namche–Barwa syntaxis, Terra Nova 9 (1997) 53–56.
[45] J. Jackson, H. Austrheim, D. McKenzie, K. Priestley, Metastability, mechanical strength, and the support of mountain belts, Geology 32 (2004) 625–628.
[46] E. Daly, C. Brown, C.P. Stark, C.J. Ebinger, Wavelet and multitaper coherence methods for assessing the elastic thickness of the Irish Atlantic margin, Geophys. J. Int. (2004), doi:10.1111/j.1365-246X.2004.02427.x.
[47] C. Braitenberg, Y. Wang, J. Fang, H. Hsu, Spatial variations of flexure parameters over the Tibet–Quinghai plateau, Earth Planet. Sci. Lett. 205 (2003) 211–224.
[48] X. Jiang, Y. Jin, M.K. McNutt, Lithospheric deformation beneath the Altyn Tagh and West Kunlun faults from recent gravity surveys, J. Geophys. Res. 109 (2004), doi:10.1029/2003JB002444.
[49] A. Yin, Cenozoic deformation of the Tarim basin and implications for mountain building in the Tibetan plateau and the Tian Shan, Tectonics 26 (2002), doi:10.1029/2001TC001300.
[50] L. Yong, P.A. Allen, A.L. Densmore, X. Qiang, Evolution of the Longmen Shan foreland basin (Western Sichuan, China) during the late Triassic Indosinian orogeny, Basin Res. 15 (2003) 117–138.
[51] A.B. Watts, K.G. Cox, The Deccan traps: an interpretation in terms of progressive lithospheric flexure in response to a migrating load, Earth Planet. Sci. Lett. 93 (1989) 85–97.
[52] A.V. Sankran, New explanation of the geological evolution of the Indian subcontinent, Curr. Sci. 77 (1999) 331–333.
[53] F.J. Simons, R.D. van der Hilst, M.T. Zuber, Spatiospectral localization of isostatic coherence anisotropy in Australia and its relation to seismic anisotropy: implications for lithospheric deformation, J. Geophys. Res. 108 (2003), doi:10.1029/2001JB000704.
[54] J. Sutton, J.V. Watson, Architecture of the continental lithosphere, Phil. Trans. Roy. Soc. Lond. 315 (1986) 5–12.
[55] K.D. Nelson, W. Zhao, L.D. Brown, J. Kuo, J. Che, X. Liu, S.L. Klemperer, Y. Makovsky, R. Meissner, J. Mechie, R. Kind, F. Wenzel, J. Ni, J. Nabelek, C. Leshou, H. Tan, W. Wei, A.G. Jones, J. Booker, M. Unsworth, W.S.F. Kidd, M. Hauck, D. Alsdorf, A. Ross, M. Cogan, C. Wu, E. Sandvol, M. Edwards, Partially molten middle crust beneath Southern Tibet: synthesis of project INDEPTH results, Science 274 (1996) 1684–1688.
[56] L.D. Brown, W. Zhao, K.D. Nelson, M. Hauck, D. Alsdorf, A. Ross, M. Cogan, M. Clark, X. Liu, J. Che, Bright spots, structure, and magmatism in southern Tibet from in-depth seismic reflection profiling, Science 274 (1996) 1688–1690.
[57] L. Zhu, D.V. Helmberger, Moho offset across the northern margin of the Tibetan Plateau, Science 281 (1998) 1170–1172.
[58] S.F. Chen, C.J.L. Wilson, Z.L. Luo, Q.D. Deng, The evolution of the Longmen Shan foreland basin, J. Southeast Asian Earth Sci. 10 (1994) 159–186.
[59] A.S.N. Murty, H.C. Tewari, P.R. Reddy, 2-D crustal velocity structure along Hirapur–Mandla profile in central India: an update, Pure Appl. Geophys. 161 (2004) 165–184.
[60] J. Ritsema, H.J. van Heijst, J.H. Woodhouse, Global transition zone tomography, J. Geophys. Res. 109 (2004), doi:10.1029/2003JB002610.
[61] D.P. McKenzie, Some remarks on the movement of small melt fractions in the mantle, Earth Planet. Sci. Lett. 95 (1989) 53–72.
[62] E. Burov, M. Diament, The effective elastic thickness (T_e) of continental lithosphere: what does it really mean? J. Geophys. Res. 100 (1995) 3905–3927.
[63] L.H. Royden, B.C. Burchfiel, R.W. King, E. Wang, Z. Chen, F. Shen, Y. Liu, Surface deformation and lower crustal flow in eastern Tibet, Science 276 (1997) 788–790.
[64] M.K. Clark, L.H. Royden, Topographic ooze: building the eastern margin of Tibet by lower crustal flow, Geology 28 (2000) 703–706.
[65] Y. Wang, Heat flow pattern and lateral variations of lithosphere strength in China mainland: constraints on active deformation, Phys. Earth Planet. Inter. 126 (2001) 121–146.
[66] P. England, G. Houseman, Role of lithospheric strength heterogeneities in the tectonics of Tibet and neighbouring regions, Nature 315 (1985) 297–301.
[67] M.P. Searle, R.L. Simpson, R.D. Law, R.R. Parrish, D.J. Waters, The structural geometry, metamorphic and magmatic evolution of the Everest massif, high Himalaya of Nepal–South Tibet, J. Geol. Soc. (London) 160 (2003) 345–366.
[68] Q. Wang, P.Z. Zhang, J.T. Freymueller, R.B. Larson, K.M. Larson, X. Lai, X. You, Z. Niu, J. Wu, Y. Li, J. Liu, Z. Yang, Q. Chen, Present-day crustal deformation in China constrained by global positioning system measurements, Science 294 (2001) 574–577.
[69] SEAGP, South East Asia Gravity Project (1991– 1995) compiled by GETECH.
[70] A. Yin, Mode of Cenozoic east–west extension in Tibet suggesting a common origin of rifts in Asia during the Indo–Asian collision, J. Geophys. Res. 107 (2000) 21745–21759.
[71] M. Rajaram, A.P. Anand, Central Indian tectonics revisited using aeromagnetic data, Earth Planets Space 55 (2003) e1–e4.
[72] D. Sarker, M.R. Kumar, J. Saul, R. Kind, P.S. Raju, R.K. Chadha, A.K. Shukla, A receiver function perspective of the Dharwar craton (India) crustal structure, Geophys. J. Int. 160 (2003) 205–211.
[73] S. Dasgupta, P. Pande, D. Ganguly, Z. Iqbal, K. Sanyal, N.V. Venkatraman, S. Dasgupta, B. Sural, L. Harendranath, K. Mazumdar, S. Sanyal, K. Roy, L.K. Das, P.S. Misra, H. Gupta, Seismotectonic Atlas of India and its Environs, Geological Survey of India, 2000.
[74] EQS USGS, Earth Quake Hazard Program online data base, http://neic.usgs.gov/neis/epic/epic, ect html.